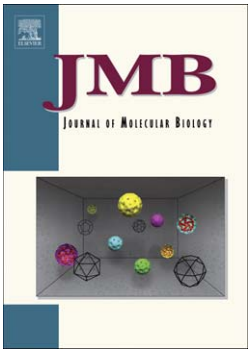

Structure and characterisation of a key epitope in the conserved C-terminal domain of the malaria vaccine candidate MSP2

Jeffrey Seow, Rodrigo A.V. Morales, Christopher A. MacRaild, Bankala Krishnarjuna, Sheena McGowan, Tamir Dingjan, Garima Jaipuria, Romain Rouet, Karyn L. Wilde, Hanudatta S. Atreya, Jack S Richards, Robin F. Anders, Daniel Christ, Nyssa Drinkwater, Raymond S. Norton

PII: S0022-2836(17)30067-0
DOI: doi:10.1016/j.jmb.2017.02.003
Reference: YJMBI 65334

To appear in: *Journal of Molecular Biology*

Received date: 16 November 2016
Revised date: 22 January 2017
Accepted date: 5 February 2017

Please cite this article as: Seow, J., Morales, R.A.V., MacRaild, C.A., Krishnarjuna, B., McGowan, S., Dingjan, T., Jaipuria, G., Rouet, R., Wilde, K.L., Atreya, H.S., Richards, J.S., Anders, R.F., Christ, D., Drinkwater, N. & Norton, R.S., Structure and characterisation of a key epitope in the conserved C-terminal domain of the malaria vaccine candidate MSP2, *Journal of Molecular Biology* (2017), doi:10.1016/j.jmb.2017.02.003

Journal of Molecular Biology

Structure and characterisation of a key epitope in the conserved C-terminal domain of the malaria vaccine candidate MSP2

Jeffrey Seow [1], Rodrigo A. V. Morales [1], Christopher A. MacRaild [1], Bankala Krishnarjuna [1], Sheena McGowan [2], Tamir Dingjan [1], Garima Jaipuria [3],Romain Rouet [4], Karyn L. Wilde [5], Hanudatta S. Atreya [3],Jack S Richards [6], Robin F. Anders [7], Daniel Christ [4], Nyssa Drinkwater [2] and Raymond S. Norton[1]

1. Monash Institute of Pharmaceutical Sciences, Monash University, Parkville, 3010, Australia
2. Department of Microbiology, Monash University, Clayton, 3168, Australia
3. NMR Research Centre, Indian Institute of Science, Bangalore, India
4. Garvan Institute of Medical Research, Darlinghurst, 2010, Australia
5. National Deuteration Facility, Australian Nuclear Science and Technology Organisation, Lucas Heights, 2234, Australia
6. Centre for Biomedical Research, The Burnet Institute, Melbourne, 3004, Australia
7. Department of Biochemistry and Genetics, La Trobe Institute for Molecular Science, La Trobe University, Melbourne, 3086, Australia

Abstract

Merozoite surface protein 2 (MSP2) is an intrinsically disordered antigen that is abundant on the surface of the malaria parasite *Plasmodium falciparum*. The two allelic families of MSP2, 3D7 and FC27, differ in their central variable regions, which are flanked by highly conserved C-terminal and N-terminal regions. In a vaccine trial, full-length 3D7 MSP2 induced a strain-specific protective immune response despite the detectable presence of conserved region antibodies. This work focuses on the conserved C-terminal region of MSP2, which includes the only disulfide bond in the protein and encompasses key epitopes recognised by the mouse monoclonal antibodies (mAb) 4D11 and 9H4. Although the 4D11 and 9H4 epitopes are overlapping, immunofluorescence assays have shown that the mAb 4D11 binds to MSP2 on the merozoite surface with a much stronger signal than 9H4. Understanding the structural basis for this antigenic difference between these antibodies will help direct the design of a broad-spectrum MSP2-based malaria vaccine. 4D11 and 9H4 were re-engineered into antibody fragments (scFv and Fv) and validated as suitable models for their full-size IgG counterparts by surface plasmon resonance and isothermal titration calorimetry. An alanine scan of the 13-residue epitope 3D7-MSP2$_{207\text{-}222}$ identified the minimal binding epitope of 4D11 and the key residues involved in binding. A 2.2 Å crystal structure of 4D11 Fv bound to the 8-residue epitope NKENCGAA provided valuable insight into the possible conformation of the C-terminal region of MSP2 on the parasite. This work underpins continued efforts to optimise recombinant MSP2 constructs for evaluation as potential vaccine candidates.

Introduction

Development of a malaria vaccine is a high priority. The mosquito-borne disease, caused by protozoa of the *Plasmodium* genus, is responsible for 200 million cases and over 430,000 deaths per year [1]. Although vector control and drug interventions have significantly decreased mortality over the past decade, the global eradication of malaria calls for a robust and effective vaccine [2]. The most advanced vaccine candidate is RTS,S/AS01, a pre-erythrocytic vaccine that has shown only modest efficacy in young children and infants in Phase III trials [3]. Blood-stage vaccines are aimed at inhibiting parasite growth and proliferation, thereby reducing the severity of symptoms and in turn mortality [4,5]. The eradication of malaria will require the development of multi-stage vaccines able to prevent blood-stage infection and block transmission.

Merozoite surface protein 2 (MSP2) is a ~23-kDa glycosylphosphatidyl inositol (GPI)-anchored protein present in the asexual blood-stages of *Plasmodium falciparum* and is one of the most abundant proteins on the surface of the merozoite [6,7]. The protein is highly polymorphic, particularly in the central variable region, which consists of tandemly arrayed repeat sequences and dimorphic sequences that differentiate the protein into two allelic families, 3D7 and FC27 (**Figure 1a**) [8,9]. The central variable region is flanked by a highly conserved 25-residue N- and ~50-residue C-terminal region, the latter containing the only disulfide bond of the protein. Similar to many other blood-stage antigens [10–12], MSP2 is an intrinsically disordered protein lacking a well-defined structure in solution [13], although the protein has been found to have a propensity for amyloid-like fibril formation [14,15]. The structural characteristics of MSP2 when interacting with the merozoite surface and those mediated by the GPI-anchor are still being explored. NMR studies have shown that the conserved N-terminal region adopts an α-helical conformation when in the presence of lipid [16] and identified some motional restriction in the conserved C-terminal region caused by the single disulfide bond [13].

MSP2 is well characterised as a vaccine candidate and has been included in several human vaccine trials [17–21]. In Phase I-IIb trials recombinant 3D7-MSP2 in combination with MSP1 and RESA was tested in Papua New Guinean children [18,22]. A 62% reduction in parasite densities was observed, although this was biased towards parasites expressing the 3D7 allele of MSP2 that was used in the vaccine [19]. This implies that the response to MSP2 dominated the protective effect

in this trial, but that the MSP2 response was highly strain-specific. A vaccine containing recombinant forms of both 3D7 and FC27 MSP2 was tested in Phase I trials and induced antibodies against both alleles that were able to inhibit parasite growth by antibody-dependant cellular inhibition (ACDI) [20] and complement-mediated inhibition [23]. A recent approach to circumvent the problems of strain-specific immune responses involved the use of MSP2 chimeras that incorporated conserved and variable regions of the 3D7 and FC27 alleles [24]. In mice, these chimeras were able to induce a robust anti-MSP2 antibody response across both alleles. Nonetheless, the success of an MSP2 vaccine is likely to be significantly enhanced by a protective immune response targeting conserved epitopes.

A panel of monoclonal antibodies (mAbs) has been generated from mice immunised with recombinant forms of both 3D7 and FC27 MSP2 [25]. Epitope mapping was performed using an array of overlapping 13-residue peptides spanning both alleles of MSP2. Overall, ten mAbs were able to recognise linear epitopes in both conserved and variable regions of MSP2. Here we focus on mAbs 4D11, 9G8 and 9H4, which recognise overlapping epitopes within an 18-residue stretch of the conserved C-terminal region encompassing the single disulfide bond. These antibodies are all able to recognise recombinant MSP2, but they show differing reactivity by immunofluorescence assays (IFA) and western blot towards MSP2 derived from parasite material. 4D11 and 9G8 exhibited a 10-fold stronger signal by IFA in comparison to 9H4, suggesting that the 9H4 epitope is less accessible on the merozoite surface. In this work we use the 4D11 mAb to better understand the structural determinants of binding to parasite MSP2.

Results

Alanine scan of 4D11 epitope

In previous work [25] the epitope of mAb 4D11 was mapped with an array of 13-residue peptides covering full-length 3D7-MSP2 and FC27-MSP2, with an overlap of 8 residues; mAb 4D11 was able to bind three of these overlapping peptides (**Figure 1b**). As the 8-residue sequence NKENCGAA was common to these three peptides this 8-mer appears to be the minimal epitope for mAb 4D11. Binding of mAb 4D11 to MSP2 was independent of the presence of the disulfide bond as the 3D7-MSP2$_{212\text{-}224}$ and 3D7-MSP2$_{215\text{-}227}$ peptides each contained only a single cysteine, and this result was confirmed in the context of full-length MSP2.

To determine the contributions to binding of each residue in the minimal epitope sequence, an alanine scan was performed of $MSP2_{207-222}$ (**Table 1**). All peptides were oxidised to form the disulfide bond before high-performance liquid chromatography (HPLC) purification. The N- and C-termini were capped by acetyl and amide moieties, respectively, to avoid electrostatic interactions with the epitope that would not be present in the full-length protein. The affinities of these peptides for 4D11 IgG were determined by SPR competition assays using immobilised 3D7 MSP2 and varying concentrations of peptide with 4D11 IgG. Direct binding assays were not suitable as the small peptide size gave a poor response. Mutations to Lys216, Glu217, Asn218 and Gly220 caused a marked decrease in binding affinity, suggesting they make key interactions with 4D11 (**Figure 1c, 1d and Supplementary Data, Figure S1**). Mutation of Glu217 to alanine resulted in a complete loss of binding. In contrast, mutation of residues 207-215 did not have a significant effect on binding. The decreased binding caused by mutation of Gly220 was unexpected but may indicate that the flexibility and/or small size of this residue are important for binding.

4D11 antibody fragments are suitable models for their full IgG counterparts

To better understand the antibody-bound conformation of the key 4D11 epitope, Fv and scFv antibody fragments were designed based on the 4D11 IgG sequence and were expressed at high yield in *Escherichia coli* [26,27]. To confirm that these antibody fragments were suitable models for 4D11 IgG, isothermal titration calorimetry (ITC) was used to compare their affinities using the 3D7-$MSP2_{207-222}$ peptide **(Supplementary Data, Figure S2)**. 4D11 Fv and scFv were found to have K_d values of 2.7 and 3.0 µM, respectively, very close to the binding affinity of 4D11 IgG at 2.2 µM.

NMR spectroscopy of $MSP2_{207-224}$ bound to 4D11 scFv

To further explore the interaction between 4D11 and MSP2, NMR was employed. To enable efficient isotope labelling, a recombinant form of 18-residue $MSP2_{207-224}$ was used. The NMR spectra of $MSP2_{207-224}$ free in solution reveal limited chemical shift dispersion, consistent with the expected lack of well-ordered structure in the free epitope **(Supplementary Data, Figure S3)**. Upon addition of a small excess of unlabelled 4D11 scFv to ^{15}N-labelled 3D7-$MSP2_{207-224}$, a more dispersed set of

peaks appeared, indicating that much of the 18-residue peptide adopts a more defined structure in the presence of the antibody. Indeed, each peak in the [^{1}H,^{15}N]-HSQC spectrum of the free peptide was significantly perturbed by antibody binding, despite the inference from the alanine scan that the N-terminal half of the peptide does not make significant interactions with the antibody. There is, however, significant variation in the peak intensity and linewidth in the antibody-bound spectra, suggesting that some parts of the peptide retain significant flexibility when bound. The relaxation properties of this complex were such that obtaining good-quality triple-resonance data from much of the bound peptide proved impossible. Accordingly, we were unable to fully assign the spectra of the bound peptide.

Crystal structure of 3D7 MSP2$_{215\text{-}222}$ bound to 4D11 Fv

Initial crystallisation trials involving 4D11 Fv in complex with the 16-residue disulfide-cyclised 3D7-MSP2$_{207\text{-}222}$ were unsuccessful. This was probably a consequence of significant flexibility in a large portion of the peptide, as inferred from the NMR data. Smaller peptides were therefore tested, including the 8-residue 3D7-MSP2$_{215\text{-}222}$, the minimal binding epitope of 4D11. The 4D11 3D7-MSP2$_{215\text{-}222}$ complex was crystallised and its structure was determined to 2.2 Å resolution (**Table 2, Figure 2**). The crystals contained four Fv-peptide complexes in the asymmetric unit, with the peptide forming two homodimers via disulfide bonds formed between the free cysteines in the monomer sequence. The bound peptide is stabilised as a β-bend ribbon, a subtype of the 3_{10} α-helical structure, which is characterised by consecutive overlapping β-turns. The first turn encompasses Asn215 (i) - Asn218 (i+3), with dihedral angles typical of a type I β-turn. The second overlapping turn encompasses Glu217 (i) – Gly220 (i+3) and, although slightly different from the canonical dihedral angles, most closely resembles a type I' β-turn [28]. The crystal structure supports the results from the alanine scan, with Lys216, Glu217 and Asn218 forming key interactions with the 4D11 V_H complementary determining regions (CDRs). Gly220 formed a hydrogen bond with a light chain Asn residue (Asn34$_L$; the Kabat numbering system was used for 4D11 residues [29] with the chain indicated by a subscript). The lack of space surrounding the Gly α-carbon explains why mutation to an alanine in this position had a detrimental effect on binding. An additional interaction was also present between the backbones of Ala221 and Gly91$_L$.

Although the peptide was purified as a monomer by HPLC, and size-exclusion chromatography confirmed that the 4D11 Fv-peptide complex was monomeric prior to crystallisation **(Supplementary Data, Figure S4)**, the 8-residue peptide 3D7-MSP2$_{215-222}$ formed a disulfide-mediated homo-dimer in the crystal. The four Fvs and peptides in the asymmetric unit of the crystal were oriented in such a way that two Fvs had their antigen-binding sites facing each other, forming a small pocket in which the peptide homo-dimer was bound (**Figure 3**). Attempts to crystallise 4D11 Fv with 8-residue monomeric peptide analogues with serine in place of the cysteine failed. The tight packing of the Fv-peptide dimer in the crystal suggests that formation of the dimer may have assisted crystal formation. The peptide dimer itself contains both intra- and intermolecular hydrogen bonds that stabilise its conformation. Asn215 in particular forms intermolecular hydrogen bonds with the backbone of Cys219 and Ala221, and an intramolecular hydrogen bond with Asn218. 4D11 binds recombinant, full-length MSP2, in which Cys219 is engaged in an intramolecular disulfide with Cys211, as a monomer and binds equally well to a cysteine mutant C219S [25]. There is no evidence that native MSP2 exists as a covalent dimer on the parasite surface [14], implying that 4D11 recognises monomeric MSP2 on the parasite surface. Accordingly, it was necessary to establish the relevance of the dimer structure to that interaction.

Dimeric 8-mer is able to bind 4D11 and 9G8 IgG

The binding affinity of dimeric 3D7-MSP2$_{215-222}$ to 4D11 IgG was determined in order to assess the relevance of the bound dimeric conformation revealed in the crystal structure. Both air oxidation and iodine oxidation of monomeric 8-mer peptide in solution failed to yield dimeric peptide. Instead, the dimer was synthesised on resin with cystine as a building block. The affinities of the monomeric and dimeric peptides were measured against both 4D11 and 9G8 IgG by an SPR competition binding assay. The affinity (K_d) of the monomeric 8-mer was 4.3 µM, slightly weaker than the dimer, at 1.4 µM. These affinities are comparable to the 0.9 µM K_d of the longer 3D7-MSP2$_{207-222}$ peptide, which contains the native disulfide bond. In addition, mAb 9G8, another antibody able to recognise parasite MSP2 by IFA and western blotting, was able to bind the monomeric and dimeric peptide with K_d values of 0.3 and 0.2 µM, respectively **(Figure 4, Supplementary Data, Figure S5)**. The ability of the dimer to bind both 4D11 IgG and 9G8 IgG at affinities comparable to those of the monomer

indicates that the conformation adopted by the bound dimer is accessible to recombinant and parasite MSP2. The slightly higher affinity binding of dimer to both antibodies suggests that the constraints imposed by the additional inter-molecular hydrogen bonds in the dimer structure are favourable for 4D11 binding, probably by reducing the entropic penalty associated with the disordered-to-ordered conformational transition upon binding.

Molecular dynamics simulations with bound 8-mer and modelled 16-mer epitopes

Molecular dynamics (MD) simulations were employed to gauge the stability of the 8-residue and 16-residue MSP2 epitopes in complex with 4D11 Fv. This enabled us to assess whether additional adjacent residues and/or the disulfide bond in the native epitope have an effect on the epitope binding conformation. MD simulations over 100 ns were performed to sample the conformational space of two peptides, $MSP2_{215-222}$ and $MSP2_{207-222}$, bound to 4D11 Fv. For the monomeric 8-residue epitope $MSP2_{215-222}$, the starting structure was extracted directly from the crystal structure. For the 16-residue epitope, the crystallographic conformation was extended N-terminally to residue 207 ($MSP2_{207-222}$), with the native disulfide modelled in. When only 4D11 Fv was aligned, the epitope RMSD for both peptides remained below 3 Å, suggesting that they remained in the binding pocket the entire simulation (**Supplementary Data, Figure S6)**. When the 8-residue epitope was aligned over this period, the epitope RMSD remained at 2 Å throughout the simulation, suggesting that the overall epitope conformation did not change significantly during simulation (**Figure 5**). As expected from the NMR data, the flexible N-terminal extensions of the modelled 16-residue epitope had a higher epitope-aligned RMSD (3 Å) than the 8-residue epitope (2 Å). However, when only the core binding residues (NKENCGAA) were used for alignment in the modelled 16-residue epitope, they were found to be stable, with an RMSD of 2 Å, identical to that of the 8-residue epitope alone. These simulations showed that the 8-residue epitope and the extended disulfide bridged 16-residue epitope share identical conformational behaviour and stability when bound to 4D11 Fv, further supporting the relevance of the bound dimeric conformation in the crystal structure.

Discussion

Intrinsically disordered proteins are known to be abundant in eukaryotic pathogens, with apicomplexans, including the malaria parasite *Plasmodium*, being particularly enriched [10,30]. Moreover, these disordered proteins are frequently targets of host immune recognition [12,31]. The effects of conformational disorder on antigenicity, and the broader implications for vaccine development, are largely unknown and are still being explored. Entropic costs associated with antibody binding to disordered antigens have been thought to be detrimental to development of high affinity and specific antibodies. However, a comparison of antibody binding to disordered and ordered antigens has shown that disordered epitopes, although usually shorter in length than their ordered counterparts, are highly efficient in their binding [31].

The recombinant form of MSP2 used in clinical trials is highly disordered [13] and the conformations of some regions of the protein differ from that of the native GPI-anchored antigen. Many disordered proteins are known to undergo a disorder-to-order transition when binding to their functional targets [32–34], and given the abundance of proteins in the merozoite surface coat it is likely that such protein-protein interactions may influence the conformation of MSP2. Additionally, it is possible that lipid interactions or the C-terminal GPI-anchor may impose conformational constraints on the protein, favouring a more ordered conformation for the parasite protein. For example, the N-terminal region of MSP2 has been found to adopt an α-helical conformation upon interaction with lipid micelles [16]. The mAb 6D8, which recognizes an epitope within the conserved N-terminal region of MSP2, is unable to recognize parasite MSP2. The structural basis for this significant difference in binding was revealed by a high-resolution crystal structure of the 6D8-epitope complex, which showed that the antibody-bound and lipid-bound conformations were incompatible [35].

The strain specificity of the vaccine response towards MSP2 implies that epitopes within the variable region play a role in protection [19]. For the development of a strain-transcending MSP2-based vaccine, however, directing the immune response towards conserved regions of the protein would be beneficial, provided that epitopes in these conserved regions are recognised by antibodies elicited by the vaccine. Thus, mAb 4D11 and its corresponding scFv and Fv antibody fragments, which recognise an epitope that is accessible in parasite MSP2, present a valuable opportunity to understand how the C-terminal conserved region behaves on the merozoite surface. The crystal structure obtained here revealed that the bound 4D11

epitope adopted a β-bend ribbon conformation with two overlapping hydrogen bonded β-turns. MD simulations showed that this conformation was stable in the context of the extended $MSP2_{207-222}$ epitope, which includes the native intramolecular disulfide bond.

The accessibility of the 4D11 epitope on the parasite surface contrasts with poor accessibility of the epitope recognised by mAb 9H4 [25]. Although 9H4 recognises an epitope that overlaps with that of 4D11, 9H4 only weakly recognises parasite MSP2 by IFA and western blotting. The ability to direct the immune response towards epitopes that are accessible on the parasite surface, such as the 4D11 epitope investigated here, and away from potentially distracting epitopes such as 9H4, suggests a strategy for engineering a more effective MSP2-based vaccine.

The alanine-scan data presented in this paper, together with the crystal structure of the bound conformation of the minimal epitope, provide a rational basis for such antigen engineering. A possible approach to optimising the immunogenicity of the C-terminal region of MSP2 involves constraining the conformation towards that observed for this key epitope in the crystal structure. Although this has not been attempted with a disordered antigen such as MSP2, there has been success in the rational design of vaccines based on structure [36–38]. In the case of MSP2, the ability of 8-residue dimer to bind to two mAbs able to recognise the parasite surface, 4D11 and 9G8, may make it a promising candidate for further study when coupled to a suitable carrier. In addition, the elimination of epitopes unlikely to contribute to protection, such as the 9H4 epitope, may improve vaccine efficacy. Currently, MSP2 analogues without the 9H4 epitope have been designed for immunisation trials in mice. The results obtained here increase our understanding of the conserved C-terminal region of MSP2 and will assist in the design of MSP2-based vaccine components that more closely match the conformational and antigenic properties of parasite MSP2.

Methods

Recombinant expression and purification of 3D7-MSP2 and $MSP2_{207-224}$

3D7-MSP2 and the C-terminal region peptide $MSP2_{207-224}$ were produced recombinantly in *E. coli* BL21(DE3) Gold (Stratagene) cells using a codon-optimised construct (Genscript) cloned into a thioredoxin-His_6 expression system, pET32a

(Novagen). The protein was expressed and purified using methods specific for recombinantly expressed disordered proteins, as described previously [30].

Antibody fragment preparation and purification

4D11 scFv and Fv antibody fragments were assembled using 4D11 V_H and V_L sequences optimised for expression in *E. coli* BL21-Gold as described previously [26]. Synthetic genes (Genscript) were cloned into pET12a (Merck Millipore) for periplasmic expression in *E. coli*. Seed culture was grown overnight in the presence of tetracycline (15 µg/mL), ampicillin (100 µg/mL) and 4% glucose. The overnight culture was diluted 1000-fold with fresh LB medium containing AMP, TET and 4% glucose at 37°C to an OD_{600} of 0.8-1.0. The cells were then pelleted (5000 g for 15 min at 4°C) and re-suspended in fresh LB medium containing AMP and TET with no glucose. After the cells were equilibrated in fresh media for 2 h, isopropyl β-D-1-thiogalactopyranoside was added to a final concentration of 1 mM to induce expression. The induced cells were incubated at room temperature overnight, then harvested by centrifugation. The protein was extracted from the periplasm by osmotic shock with treatment of sucrose buffer (30 mM Tris, 2 mM EDTA, 30% sucrose, pH 8.0) followed by lysis of the periplasm with 5 mM $MgCl_2$ and 10 µg/mL DNase I at 4°C.

The 4D11 antibody fragment was purified from the periplasmic extract by affinity purification using 3D7 MSP2-bound beads. The MSP2 affinity column was prepared by amide conjugation of full-length 3D7 MSP2 to hydroxysuccimidyl-Sepharose resin (Sigma-Aldrich) following the manufacturer's protocol. Bound antibody fragments were washed extensively with 50 mM phosphate buffer, pH 7, and eluted from the MSP2 beads with 100 mM glycine, pH 2.7. Samples were neutralized immediately with 1M Tris, concentrated in a 10 kDa MWCO centrifuge filter (Amicon Ultra-0.5, Merck-Millipore) and dialyzed against 20 mM ammonium bicarbonate prior to lyophilization and storage at -80 ºC. The purity of each antibody fragment was assessed by SDS-PAGE and LC-MS.

Peptide synthesis

Peptides including the alanine scan of 3D7-$MSP2_{207-222}$, $MSP2_{215-222}$ along with the corresponding 8-residue monomeric analogues $MSP2_{215-222}$(C219S) and $MSP2_{215-}$

$_{222}$(C219α-aminobutyric acid) were synthesised in-house by standard 9-fluorenylmethoxycarbonyl (FMOC) solid phase chemistry using an automated peptide synthesiser 3 (PS3, Pti Instruments). The peptides were assembled via coupling of 0.3 mmol (3 equiv) of FMOC-protected amino acids to 0.1 mmol rink amide AM resin (0.53 mmol/g loading). Coupling reactions were carried out for 50 min under the activation of 0.3 mmol (3 equiv) O-(1H-6-chlorobenzotriazole-1-yl)-1,1,3,3-tetramethyluronium hexafluorophosphate (HCTU) and 0.6 mmol (6 equiv) N,N-diisopropylethylamine (DIPEA). A double coupling was performed on the first residue of each peptide. Chain deprotection was carried out with 20% piperidine in DMF for 2 min. The peptides were N-terminally capped with an acetyl moiety using 0.5 mmol (5 equiv) of acetic anhydride in 0.5 mmol (5 equiv) DIPEA. Dimerization of the MSP2$_{215\text{-}222}$ peptide proved difficult as conventional air oxidation over 5 days and iodine oxidation over 24 h were unsuccessful. Instead the dimeric peptide was synthesised on resin using bis-FMOC-L-cystine and constructed by fragment condensation.

Cleavage of the complete peptides was performed with TFA:TIPS:water (95:2.5:2.5 v/v). The cleaved material was precipitated in cold diethyl ether overnight at -20 ºC. The insoluble peptide material was spun down at 4,000 rpm for 30 min at 0 ºC and the pellet washed twice in cold diethyl ether prior to removal of the organic phase. The crude peptide mixture was resuspended in 50% acetonitrile/0.1% TFA, filtered and freeze-dried prior to further purification. Disulfide bond-containing peptides were oxidised by air in 100 mM ammonium bicarbonate for 2 h before HPLC purification. MSP2 peptides were purified on a reverse-phase C18 column (Zorbax, 10 x 300 mm) using a linear gradient of 5 to 60% of solvent B (80% acetonitrile / 9.9% water / 0.1% TFA) against solvent A (0.1% TFA in water) over 1 h. The purity of MSP2 peptides was assessed by mass spectrometry (LC-MS) **(Supplementary Data, Figures S7, S8 and S9)**.

Affinity measurements

The affinities of 4D11 IgG and Fv for synthetic peptides and recombinant MSP2 were determined by ITC (Microcal ITC-200, GE Healthcare) using murine mAb 6D8, 6D8 scFv or 6D8 Fv. Titrations were performed in 10 mM HEPES, 100 mM NaCl, pH 7.4 at 25°C. Antibody concentrations were 10 µM (IgG) or 20 µM (scFv/Fv), with peptide titrated from 200 µM stocks. Control titrations of peptide into buffer were performed,

and resulting heats of dilution subtracted from the corresponding titration into antibody. Affinities for peptide epitopes and full-length 3D7-MSP2 to 4D11 IgG were measured by SPR (Biacore T200, GE Healthcare) using a Mouse Antibody Capture kit (GE Healthcare). Initial direct binding SPR assays with the alanine scan peptides were not feasible due to sensitivity issues caused by the small size of the peptides. Instead, affinities were measured by an SPR competition assay with 3D7-MSP2 immobilised on a CM5 chip. A standard curve was established by flowing eight 2-fold dilutions of 4D11 IgG from 100 nM stock. Varying 3-fold dilutions of peptide were used from 10 µM stock to compete with the immobilised antigen. 50 nM 4D11 IgG was used throughout the assay.

X-ray data collection and structure refinement

4D11 Fv and synthetic peptide 3D7-MSP2$_{215\text{-}222}$ were mixed at 1:1.5 (mol/mol) ratio in crystallization buffer (20 mM Tris-HCl, 100 mM NaCl, pH 7.0) for 1 h at room temperature. Unbound peptide and high molecular weight aggregates were removed by gel filtration (Superdex 75 10/300 GL, GE Healthcare). The complex was concentrated to 20-30 mg/mL by gentle centrifugation (Amicon Ultra 3 kDa, Merck-Millipore Pty) and cleared of precipitants by centrifugation at 10,000 rpm for 10 min, then filtered through a 0.22 µm spin filter at 4ºC. Antibody concentrations were determined based on the absorbance at 280 nm ($A^{1\%}_{280nm}$ = 1.6) by NanoDrop (Thermo-Fisher Pty Ltd).

Crystals were grown using the hanging-drop vapour diffusion method, with 1:1 (vol/vol) ratio of protein to reservoir solution and 0.5 mL well volume. Crystals grew in 23% (w/v) PEG3350, 0.1 M BIS Tris (pH 6.0), 0.2 M $MgCl_2$ and were cryo-protected by the addition of 10 % glycerol prior to data collection. Data were collected at 100 K using the Australian synchrotron macro crystallography MX1 beamline 3BM1 [39] Data was processed using the CCP4 suite [40]. Diffraction images were indexed and integrated using iMosfilm and Aimless was used to merge data sets and perform scale and average. The final structure was solved with merged data from two crystals collected under identical conditions. 5% of each dataset was flagged for calculation of R_{Free} [41]. Structure determination proceeded using the Molecular Replacement method and the program PHASER [42]. A search model was constructed from the crystal structure of mouse Fv 6D8 (PDB ID 4QYO) by removing the ligand from the search model and mutation of residues to the 4D11

sequence using CHAINSAW from the CCP4 suite [40]. Initial electron density maps clearly showed unbiased features of the 3D7-MSP2$_{215-222}$ peptide ligand between the two protein chains. All subsequent model building and structural validation was undertaken using Phenix [43,44] and COOT [45]. The refined 2Fo–Fc electron density of the 3D7-MSP2$_{215-222}$ peptide ligand is shown in **Supplementary Data, Figure S10**. Solvent molecules were added only if they had acceptable hydrogen-bonding geometry contacts of 2.5 to 3.5 Å with protein atoms or with existing solvent and were in good $2F_o$-F_c and F_o-F_c electron density. Molprobity was used to assess the quality of the refined structure [46].

MD simulations

Molecular dynamics simulation was employed to gauge the stability of the 8-residue and 16-residue MSP2 epitopes in complex with 4D11 Fv. The initial models of the 16-residue disulfide-bonded epitope MSP2$_{207-222}$ were created using Modeller version 9.17 [47], with the 8-residue epitope from the crystal structure as a template. A total of 30 models was prepared, those with disfavoured rotamers and dihedral angles were removed, and a single model was chosen as a starting point for further molecular dynamic studies. The simulations and analysis of 4D11 Fv in complex with both the monomeric 8-residue epitope and the modelled 16-residue disulfide-bonded peptide were performed using GROMACS version 5.1.2 software [48,49] and Amber 99SB-ILDN force field [50]. The protonation state of ionisable amino acids was set for a pH of 7.0, with Na^+ or Cl^- counterions added to neutralize the system as required. The complex was placed in a rhombic dodecahedron box with a minimal distance between protein and the wall of the unit cell set to 10 Å, and solvated using the TIP3P water model. The solvated system was minimized using the steepest descent algorithm for 5000 steps. The system was equilibrated in three stages: first, a 100 ps MD simulation at 10 K with positional restraints on the protein (1000 kJ/mol-nm^2) in an NVT ensemble. The V-rescale modified Berendsen thermostat with a time coupling constant of 0.1 ps was used for temperature regulation [51]. This simulation was then repeated with no restraints. Finally, the system was equilibrated at 300 K for 100 ps in an NPT ensemble. The Parinello-Rahman barostat with a pressure coupling constant of 2 ps was used to control system pressure [52]. The LINCS algorithm was used to constrain covalent bonds, allowing a simulation time step of 2 fs [48]. A non-bonded interaction cutoff of 9 Å was used. Long range electrostatics

were calculated with the particle mesh Ewald (PME) method [53].The production simulations were performed in an NPT ensemble at 300 K and 1 bar for 100 ns. Snapshots were stored every 2 ps resulting in a total of 50000 conformations which were used in the MD trajectory analysis. Post-processing of the MD simulations was performed using the GROMACS utility *rmsdist*.

Accession numbers

Coordinates and structure factors have been deposited in the Protein Data Bank with accession number 5TBD. Nucleotide sequences of the 4D11 V_H and V_L chain have been deposited to the Genbank database (KY038039 and KY03040, respectively).

Acknowledgments

We thank David Zahra for his assistance in sequencing mAbs 4D11 and 9H4 and design of antibody fragments. R.S.N. acknowledges fellowship support from the National Health and Medical Research Council of Australia. This work was supported in part by the Australian Government Research Training Program Scholarship and the National Health and Medical Research Council (project grant 1042520). We thank the Australian Synchrotron for beam time (MXCAP 8208) and technical assistance. The National Deuteration Facility is partially funded by the National Collaborative Research Infrastructure Strategy, an initiative of the Australian Federal Government.

Abbreviations used: ACDI, antibody-dependant cellular inhibition; CDR, complementary determining region; Fv, variable fragment; GPI, glycosylphosphatidyl inositol; HPLC, high-performance liquid chromatography; IFA, immunofluorescence assays; ITC, isothermal titration calorimetry; mAb, monoclonal antibody; MD, molecular dynamics; MSP2, Merozoite surface protein 2; scFv, single chain variable fragment; SPR, surface plasmon resonance; V_H, variable heavy chain; V_L, variable light chain

References

[1] WHO, World Malaria Report 2015, WHO Press, Geneva, Switzerland (2015).

[2] C.J.L. Murray, L.C. Rosenfeld, S.S. Lim, K.G. Andrews, K.J. Foreman, D. Haring, et al., Global malaria mortality between 1980 and 2010: a systematic analysis., Lancet. **379** 413–31 (2012).

[3] B.M. Greenwood, Efficacy and safety of RTS,S/AS01 malaria vaccine with or without a booster dose in infants and children in Africa : final results of a phase 3, individually randomised, controlled trial, Lancet. **386** 31-45 (2015).

[4] J.S. Richards, J.G. Beeson, The future for blood-stage vaccines against malaria., Immunol. Cell Biol. **87** 377–90 (2009).

[5] L. von Seidlein, P. Bejon, Malaria vaccines: past, present and future., Arch. Dis. Child. **98** 981–5 (2013).

[6] P.R. Gilson, T. Nebl, D. Vukcevic, R.L. Moritz, T. Sargeant, T.P. Speed, et al., Identification and stoichiometry of glycosylphosphatidylinositol-anchored membrane proteins of the human malaria parasite Plasmodium falciparum., Mol. Cell. Proteomics. **5** 1286–99 (2006).

[7] P.R. Sanders, L.M. Kats, D.R. Drew, R.A. O'Donnell, M. O'Neill, A.G. Maier, et al., A set of glycosylphosphatidyl inositol-anchored membrane proteins of Plasmodium falciparum is refractory to genetic deletion., Infect. Immun. **74** 4330–8 (2006).

[8] J.A. Smythe, R.L. Coppel, K.P. Day, R.K. Martin, A.M. Oduola, D.J. Kemp, et al., Structural diversity in the Plasmodium falciparum merozoite surface antigen 2., Proc. Natl. Acad. Sci. U. S. A. **88** 1751–5 (1991).

[9] B. Fenton, J.T. Clark, C.M. Khan, J.V. Robinson, D. Walliker, R. Ridley, et al., Structural and antigenic polymorphism of the 35- to 48-kilodalton merozoite surface antigen (MSA-2) of the malaria parasite Plasmodium falciparum., Mol. Cell. Biol. **11** 963–971 (1991).

[10] Z. Feng, X. Zhang, P. Han, N. Arora, R.F. Anders, R.S. Norton, Abundance of intrinsically unstructured proteins in P. falciparum and other apicomplexan parasite proteomes., Mol. Biochem. Parasitol. **150** 256–67 (2006).

[11] S. Olugbile, C. Kulangara, G. Bang, S. Bertholet, E. Suzarte, V. Villard, et al., Vaccine potentials of an intrinsically unstructured fragment derived from the blood stage-associated Plasmodium falciparum protein PFF0165c., Infect. Immun. **77** 5701–9 (2009).

[12] A.J. Guy, V. Irani, C.A. MacRaild, R.F. Anders, R.S. Norton, J.G. Beeson, et al., Insights into the immunological properties of intrinsically disordered malaria proteins using proteome scale predictions, PLoS One. **10** 1–22 (2015).

[13] X. Zhang, M.A. Perugini, S. Yao, C.G. Adda, V.J. Murphy, A. Low, et al., Solution conformation, backbone dynamics and lipid interactions of the intrinsically unstructured malaria surface protein MSP2., J. Mol. Biol. **379** 105–21 (2008).

[14] C.G. Adda, V.J. Murphy, M. Sunde, L.J. Waddington, J. Schloegel, G.H. Talbo, et al., Plasmodium falciparum merozoite surface protein 2 is unstructured and forms amyloid-like fibrils., Mol. Biochem. Parasitol. **166** 159–71 (2009).

[15] X. Yang, C.G. Adda, C.A. MacRaild, A. Low, X. Zhang, W. Zeng, et al., Identification of key residues involved in fibril formation by the conserved N-terminal region of Plasmodium falciparum merozoite surface protein 2 (MSP2), Biochimie. **92** 1287–1295 (2010).

[16] C.A. MacRaild, M.Ø. Pedersen, R.F. Anders, R.S. Norton, Lipid interactions of the malaria antigen merozoite surface protein 2., Biochim. Biophys. Acta. **1818** 2572–8 (2012).

[17] R.F. Anders, C.G. Adda, M. Foley, R.S. Norton, Recombinant protein vaccines against the asexual blood stages of Plasmodium falciparum., Hum. Vaccin. **6** 39–53 (2010).

[18] B. Genton, F. Al-Yaman, R. Anders, A. Saul, G. Brown, D. Pye, et al., Safety and immunogenicity of a three-component blood-stage malaria vaccine in adults living in an endemic area of Papua New Guinea., Vaccine. **18** 2504–11 (2000).

[19] B. Genton, I. Betuela, I. Felger, F. Al-Yaman, R.F. Anders, A. Saul, et al., A recombinant blood-stage malaria vaccine reduces Plasmodium falciparum density and exerts selective pressure on parasite populations in a phase 1-2b trial in Papua New Guinea., J. Infect. Dis. **185** 820–7 (2002).

[20] J.S. McCarthy, J. Marjason, S. Elliott, P. Fahey, G. Bang, E. Malkin, et al., A phase 1 trial of MSP2-C1, a blood-stage malaria vaccine containing 2 isoforms of MSP2 formulated with Montanide® ISA 720., PLoS One. **6** e24413 (2011).

[21] S.D. Polley, D.J. Conway, D.R. Cavanagh, J.S. McBride, B.S. Lowe, T.N. Williams, et al., High levels of serum antibodies to merozoite surface protein 2 of Plasmodium falciparum are associated with reduced risk of clinical malaria in coastal Kenya., Vaccine. **24** 4233–46 (2006).

[22] B. Genton, F. Al-Yaman, I. Betuela, R.F. Anders, A. Saul, K. Baea, et al., Safety and immunogenicity of a three-component blood-stage malaria vaccine (MSP1, MSP2, RESA) against Plasmodium falciparum in Papua New Guinean children, Vaccine. **22** 30–41 (2003).

[23] M.J. Boyle, L. Reiling, R.F. Anders, J.G. Beeson, M.J. Boyle, L. Reiling, et al., Human Antibodies Fix Complement to Inhibit Plasmodium falciparum Invasion of Erythrocytes and Are Associated with Protection against Malaria, Immunity. **42** 580–590 (2015).

[24] B. Krishnarjuna, D. Andrew, C.A. MacRaild, R.A.V. Morales, J.G. Beeson, R.F. Anders, et al., Strain-transcending immune response generated by chimeras of the malaria vaccine candidate merozoite surface protein 2, Sci. Rep. **6** 20613 (2016).

[25] C.G. Adda, C.A. MacRaild, L. Reiling, K. Wycherley, M.J. Boyle, V. Kienzle, et al., Antigenic characterization of an intrinsically unstructured protein, Plasmodium falciparum merozoite surface protein 2., Infect. Immun. **80** 4177–85 (2012).

[26] R. Rouet, D. Lowe, K. Dudgeon, B. Roome, P. Schofield, D. Langley, et al., Expression of high-affinity human antibody fragments in bacteria., Nat. Protoc. **7** 364–73 (2012).

[27] C.M. Lee, N. Iorno, F. Sierro, D. Christ, Selection of human antibody fragments by phage display, Nat Protoc. **2** 3001–3008 (2007).

[28] E.G. Hutchinson, J.M. Thornton, A revised set of potentials for beta-turn formation in proteins., Protein Sci. **3** 2207–2216 (1994).

[29] E.A. Kabat, T. Te Wu, C. Foeller, H.M. Perry, K.S. Gottesman, Sequences of proteins of immunological interest, DIANE publishing, 1992.

[30] C.A. MacRaild, M. Zachrdla, D. Andrew, B. Krishnarjuna, J. Novacek, L. Zidek, et al., Conformational dynamics and antigenicity in the disordered malaria antigen merozoite surface protein 2, PLoS One. **10** 1–19 (2015).

[31] C.A. Macraild, J.S. Richards, R.F. Anders, R.S. Norton, Antibody Recognition of Disordered Antigens, Structure. **24** 148–157 (2016).

[32] V.N. Uversky, A.K. Dunker, Understanding protein non-folding., Biochim. Biophys. Acta. **1804** 1231–64 (2010).

[33] H.J. Dyson and P.E. Wright, Intrinsically unstructured proteins and their functions, Nat. Rev. Mol. Cell Biol. (2005).

[34] P.E. Wright, H.J. Dyson, Intrinsically disordered proteins in cellular signalling and regulation, Nat. Rev. Mol. Cell Biol. **16** 18–29 (2014).

[35] R.A. V. Morales, C.A. MacRaild, J. Seow, B. Krishnarjuna, N. Drinkwater, R. Rouet, et al., Structural basis for epitope masking and strain specificity of a conserved epitope in an intrinsically disordered malaria vaccine candidate, Sci. Rep. **5** 10103 (2015).

[36] M. Scarselli, B. Aricò, B. Brunelli, S. Savino, F. Di Marcello, E. Palumbo, et al., Rational design of a meningococcal antigen inducing broad protective immunity., Sci. Transl. Med. **3** 91ra62 (2011).

[37] J.S. McLellan, B.E. Correia, M. Chen, Y. Yang, B.S. Graham, W.R. Schief, et al., Design and characterization of epitope-scaffold immunogens that present the motavizumab epitope from respiratory syncytial virus., J. Mol. Biol. **409** 853–66 (2011).

[38] J.S. McLellan, M. Chen, M.G. Joyce, M. Sastry, G.B.E. Stewart-Jones, Y. Yang, et al., Structure-based design of a fusion glycoprotein vaccine for respiratory syncytial virus., Science. **342** 592–8 (2013).

[39] N.P. Cowieson, D. Aragao, M. Clift, D.J. Ericsson, C. Gee, S.J. Harrop, et al., MX1: A bending-magnet crystallography beamline serving both chemical and macromolecular crystallography communities at the Australian Synchrotron, J. Synchrotron Radiat. **22** 187–190 (2015).

[40] The CCP4 suite: programs for protein crystallography., Acta Crystallogr. D. Biol. Crystallogr. **50** 760–3 (1994).

[41] A.T. Brünger, Assessment of phase accuracy by cross validation: the free R value. Methods and applications., Acta Crystallogr. D. Biol. Crystallogr. **49** 24–36 (1993).

[42] A.J. McCoy, R.W. Grosse-Kunstleve, P.D. Adams, M.D. Winn, L.C. Storoni, R.J. Read, Phaser crystallographic software., J. Appl. Crystallogr. **40** 658–674 (2007).

[43] P.D. Adams, P. V Afonine, G. Bunkóczi, V.B. Chen, I.W. Davis, N. Echols, et al., PHENIX: a comprehensive Python-based system for macromolecular structure solution., Acta Crystallogr. D. Biol. Crystallogr. **66** 213–21 (2010).

[44] P. V Afonine, R.W. Grosse-Kunstleve, N. Echols, J.J. Headd, N.W. Moriarty, M. Mustyakimov, et al., Towards automated crystallographic structure refinement with phenix.refine., Acta Crystallogr. D. Biol. Crystallogr. **68** 352–67 (2012).

[45] P. Emsley, K. Cowtan, Coot: model-building tools for molecular graphics., Acta Crystallogr. D. Biol. Crystallogr. **60** 2126–32 (2004).

[46] V.B. Chen, W.B. Arendall, J.J. Headd, D.A. Keedy, R.M. Immormino, G.J. Kapral, et al., MolProbity: All-atom structure validation for macromolecular crystallography, Acta Crystallogr. Sect. D Biol. Crystallogr. **66** 12–21 (2010).

[47] B. Webb, A. Sali, Comparative Protein Structure Modeling Using Modeller, in: Curr. Protoc. Bioinforma., John Wiley & Sons, 2014: pp. 1–5.

[48] B. Hess, C. Kutzner, D. Van Der Spoel, E. Lindahl, GROMACS 4: Algorithms for highly efficient, load-balanced, and scalable molecular simulation, J. Chem. Theory Comput. **4** 435–447 (2008).

[49] S. Pronk, S. Páll, R. Schulz, P. Larsson, P. Bjelkmar, R. Apostolov, et al., GROMACS 4.5: A high-throughput and highly parallel open source molecular simulation toolkit, Bioinformatics. **29** 845–854 (2013).

[50] K. Lindorff-Larsen, S. Piana, K. Palmo, P. Maragakis, J.L. Klepeis, R.O. Dror, et al., Improved side-chain torsion potentials for the Amber ff99SB protein force field, Proteins Struct. Funct. Bioinforma. **78** 1950–1958 (2010).

[51] G. Bussi, D. Donadio, M. Parrinello, Canonical sampling through velocity rescaling, J. Chem. Phys. **126** (2007).

[52] M. Parrinello, A. Rahman, Polymorphic transitions in single crystals: A new molecular dynamics method, J. Appl. Phys. **52** 7182–7190 (1981).

[53] U. Essmann, L. Perera, M.L. Berkowitz, T. Darden, H. Lee, L.G. Pedersen, A smooth particle mesh Ewald method, J Chem Phys. **103** 8577–8593 (1995).

Figure Legends

Figure 1. (a) Schematic of the primary structures of 3D7 and FC27 MSP2. **(b)** Aligned 13-mer peptides from peptide array able to bind with mAb 4D11. 3D7-MSP2$_{212-224}$ and 3D7-MSP2$_{210-222}$ reacted strongly with mAb 4D11 by ELISA [25]. Overlapping residues are shown in bold, cysteine residues are shown in red. **(c)** SPR competition assay of alanine scan 16-mer peptides of 3D7-MSP2$_{207-222}$. Black lines show alanine mutants with no effect on binding, the green line indicates the wild-type binding of 3D7-MSP2$_{207-222}$, red lines indicate the alanine mutations that decreased the binding to 4D11 IgG. **(d)** Schematic representation of disulfide-bonded peptide sequence indicating location of key residues in red.

Figure 2. 2.2 Å crystal structure of 4D11 Fv bound to the 8-mer peptide 3D7-MSP2$_{215-222}$. **(a)** Crystal structure of 3D7-MSP2$_{215-222}$ bound within the paratope of 4D11 Fv **(b)** The conformation of 3D7-MSP2$_{215-222}$ (orange) is stabilised by a number of hydrogen bond interactions (shown as green dashed lines) with the CDRs of 4D11 Fv (grey) involving residues Lys216, Glu217, Asn218, Gly220 and Ala221.

Figure 3. Crystal structure of 4D11 Fv in complex with 3D7-MSP2$_{215-222}$ homodimer **(a)** Both peptides in the homodimer are able to bind to 4D11 Fv, hence the unusual orientation of two Fvs facing towards each other. **(b)** Hydrogen bond interactions within the homodimer include intramolecular (black dashed lines) and intermolecular (green dashed lines)

Figure 4. SPR competition assay of dimeric and monomeric 8-mer peptide 3D7-MSP2$_{215-222}$ using immobilised C-terminal region peptide 3D7-MSP2$_{171-221}$, **(a)** 4D11 IgG **(b)** 9G8 IgG

Figure 5. Root mean square deviation (RMSD) of the epitope shape over 100 ns with respect to the equilibrated MD simulation starting conformation. All residues were aligned for the 8-mer (red) and 16-mer (green), blue indicates the RMSD of the

16-mer with only the binding residues 217-222 aligned. The conformation of the binding region of the modelled 16-residue epitope does not change significantly.

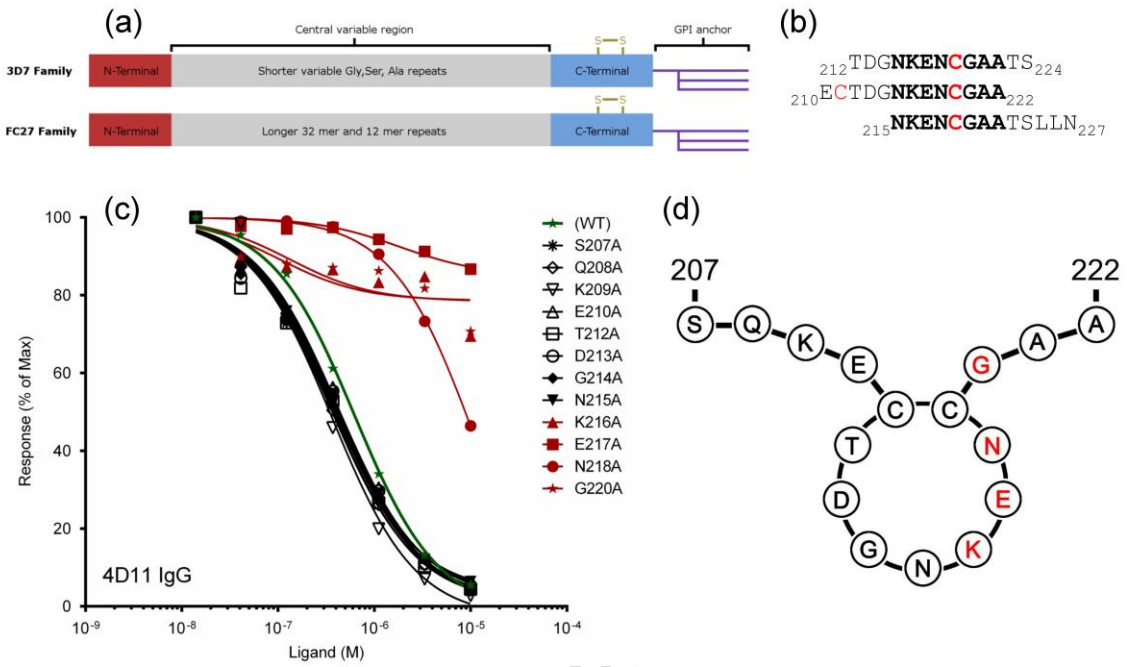

Figure 1

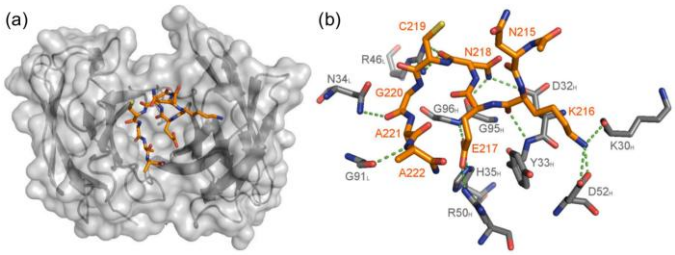

Figure 2

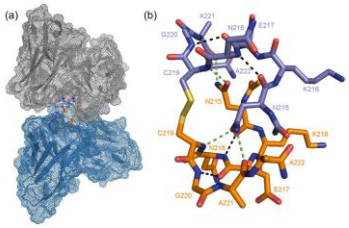

Figure 3

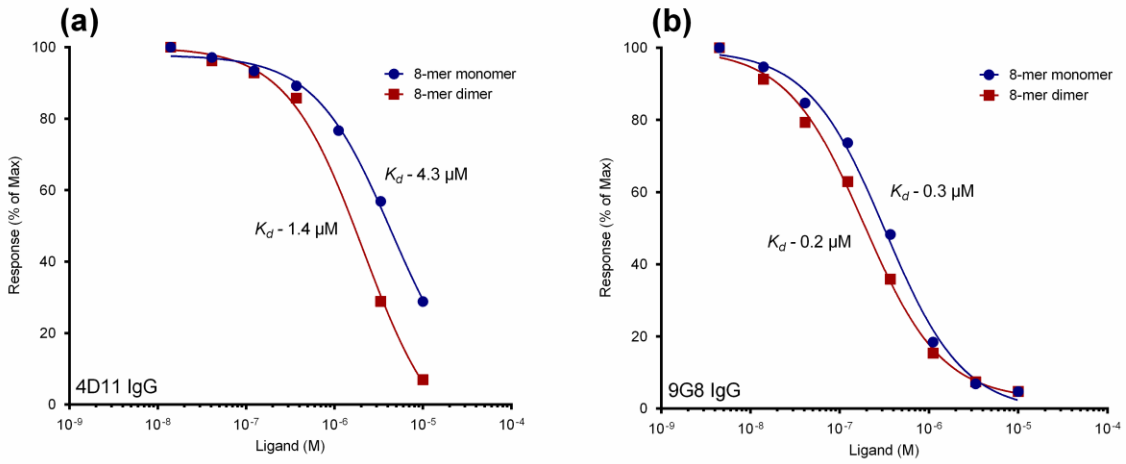

Figure 4

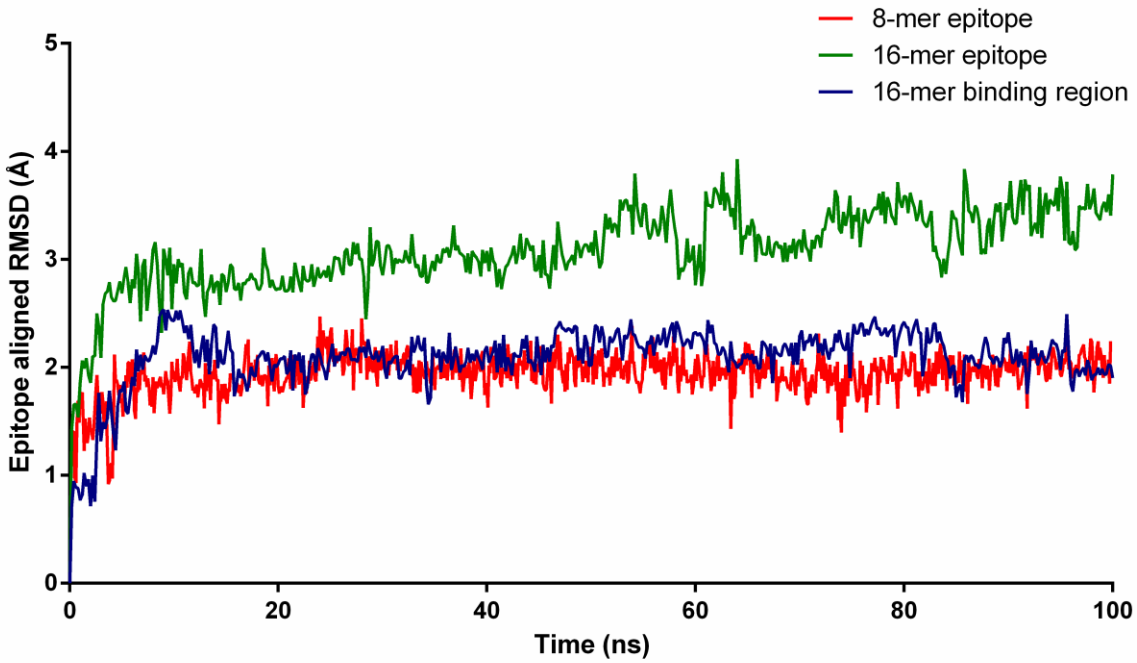

Figure 5

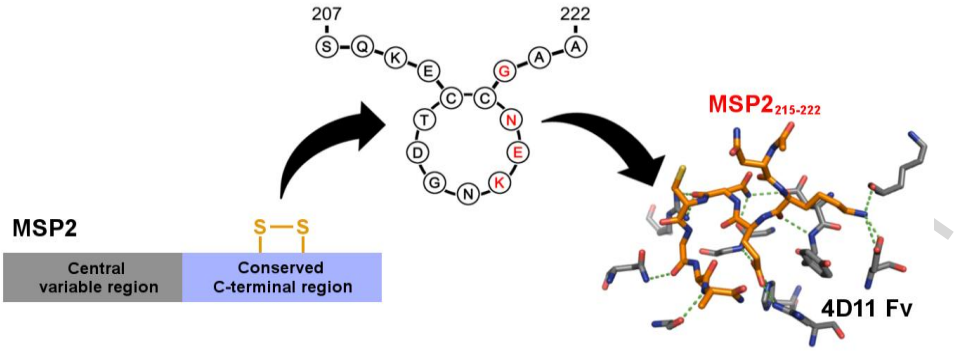

Graphical abstract

Tables

Table 1. Alanine scan of the 13-residue mAb 4D11 epitope $MSP2_{207-222}$ to determine key residues for binding. K_d was determined by SPR (± standard deviation of three replicate experiments). Synthetic peptides were N-terminally acetylated and C-terminally amidated.

Peptide	16-mer sequence*	K_d against 4D11 IgG (µM)
3D7-$MSP2_{207-222}$ (WT)	SQKECTDGNKENCGAA	0.9 ± 0.4
S207A	AQKECTDGNKENCGAA	0.5 ± 0.2
Q208A	SAKECTDGNKENCGAA	0.4 ± 0.1
K209A	SQAECTDGNKENCGAA	0.3 ± 0.1
E210A	SQKACTDGNKENCGAA	0.5 ± 0.2
T212A	SQKECADGNKENCGAA	0.5 ± 0.2
D213A	SQKECTAGNKENCGAA	0.5 ± 0.1
G214A	SQKECTDANKENCGAA	0.4 ± 0.1
N215A	SQKECTDGAKENCGAA	0.5 ± 0.2
K216A	SQKECTDGNAENCGAA	21.0 ± 6.0
E217A	SQKECTDGNKANCGAA	219 ± 64
N218A	SQKECTDGNKEACGAA	6.0 ± 2.3
G220A	SQKECTDGNKENCAAA	42 ± 10

Table 2. Data collection and refinement statistics

4D11 Fv + MSP2$_{215-222}$ (PDB ID: 5TBD)	
Data collection	
Space group	P1
Cell dimensions	
a, b, c (Å)	41.97, 72.97, 81.97
α, β, γ (°)	68.2, 78.8, 76.8
Resolution (Å)	65.99-2.2 (2.27-2.20)
R_{pim} (%)	15.5 (66.4)
I/$\boldsymbol{\sigma_I}$	7.5 (2.6)
Completeness (%)	100 (100)
Redundancy	7.3 (7.3)
Unique reflections	43777
Refinement	
Resolution	2.2
Number of reflections	321569
R_{work}/R_{free} (%)	20.66/24.70
Number of Atoms	
Protein	7064
Water	365
B-factors	
Protein	27.1
Fv	27.3
Epitope	19.9
Water	26.9
RMSDs	
Bond length (Å)	0.003
Bond angles (°)	0.68
Ramachandran Plot	
Outliers (%)	0
Favoured (%)	98.1
Rotamer Outliers (%)	0.3
Clashscore [46]	2.65

Values in parentheses refer to the highest resolution shell.
Agreement between intensities of repeated measurements of the same reflections and can be defined as: $\sum(I_{h,i} - \langle I_h \rangle)/\sum I_{h,i}$, where $I_{h,i}$ are individual values and $\langle I_h \rangle$ is the mean value of the intensity of reflection h.

Highlights

- Protective antibody response to the malaria antigen MSP2 is largely strain-specific.
- Monoclonal antibody 4D11 recognises a conserved epitope on parasite MSP2.
- Alanine scan identified the minimal binding epitope of 4D11.
- Crystal structure revealed the conformation of the 4D11-bound epitope.
- Insight into the conformation of the conserved epitope on the parasite will inform MSP2-based vaccine design.